 Related Commentary, page 2157

Angiopoietin-1 is essential in mouse vasculature during development and in response to injury

Marie Jeansson,[1] Alexander Gawlik,[2] Gregory Anderson,[3] Chengjin Li,[1] Dontscho Kerjaschki,[4] Mark Henkelman,[3] and Susan E. Quaggin[1,5]

[1]Samuel Lunenfeld Research Institute, Mount Sinai Hospital, University of Toronto, Toronto, Canada. [2]Rheinisch-Westfälische Technische Hochschule (RWTH) University of Aachen, Aachen, Germany. [3]Mouse Imaging Centre, Toronto Centre for Phenogenomics, Toronto, Canada. [4]Clinical Institute of Pathology, Medical University of Vienna, Vienna, Austria. [5]Division of Nephrology, St. Michael's Hospital, and Department of Medicine, University Health Network, University of Toronto, Toronto, Canada.

Angiopoietin-1/Tek signaling is a critical regulator of blood vessel development, with conventional knockout of angiopoietin-1 or Tek in mice being embryonically lethal due to vascular defects. In addition, angiopoietin-1 is thought to be required for the stability of mature vessels. Using a Cre-Lox conditional gene targeting approach, we have studied the role of angiopoietin-1 in embryonic and adult vasculature. We report here that angiopoietin-1 is critical for regulating both the number and diameter of developing vessels but is not required for pericyte recruitment. Cardiac-specific knockout of angiopoietin-1 reproduced the phenotype of the conventional knockout, demonstrating that the early vascular abnormalities arise from flow-dependent defects. Strikingly, deletion in the entire embryo after day E13.5 produced no immediate vascular phenotype. However, when combined with injury or microvascular stress, angiopoietin-1 deficiency resulted in profound organ damage, accelerated angiogenesis, and fibrosis. These findings redefine our understanding of the biological roles of angiopoietin-1: it is dispensable in quiescent vessels but has a powerful ability to modulate the vascular response after injury.

Introduction

Angiopoietin-1 (Angpt1) is a secreted 70-kDa glycoprotein and a member of the angiopoietin family of growth factors. Angpt1 is the major agonist for the tyrosine kinase receptor, Tek, which is found primarily on endothelial cells. Angpt1 is produced by vasculature support cells and specialized pericytes such as podocytes in the kidney and ITO cells in the liver (1). It has been suggested that Angpt1 is required to maintain endothelial cell quiescence, promoting stability through pericyte recruitment and formation of non-leaky vessels. It has also been shown that Angpt1 can restore poorly remodeled and leaky vessels (2). The Angpt/Tek pathway is critical for normal development, as conventional *Angpt1* or *Tek* knockout mice exhibit lethality between E9.5 and E12.5, with similar abnormal vascular phenotypes and loss of heart trabeculations (3–5).

Another member of the angiopoietin family, Angpt2, is a Tek antagonist that is produced and stored in Weibel-Palade bodies in endothelial cells (6). Angpt2 inhibits Tek in an autocrine fashion and promotes endothelial activation, destabilization, and inflammation (7). The precise consequences of Angpt2, with respect to angiogenesis, are dependent on the presence or absence of another key angiogenic factor, Vegfa. Dysregulation of the ANGPT/TEK system is a common feature of many disease states, characterized by vascular dysfunction, including diabetes, malaria, sepsis, and pulmonary hypertension. For example, an increased ratio of ANGPT2/ANGPT1 in serum is a powerful predictor of adverse outcomes in these conditions, suggesting a central role for this vascular signaling pathway in their pathogenesis (8–10). However, a specific causal role for dysregulated ANGPT/TEK signaling in these diseases is not clear. Furthermore, several key questions remain regarding its role(s) in vascular development and maintenance.

To address these questions and to overcome the early embryonic lethality of the conventional knockouts, we generated a mouse line with a conditional (floxed) *Angpt1* allele. Using a number of different Cre-driver strains, we performed a comprehensive analysis of phenotypes resulting from timed deletions of *Angpt1* from conception to adulthood either from all cells (using a Rosa-rtTA/tetO-Cre bitransgenic system) or from specific cell compartments in the heart and kidney. These studies have generated several surprising findings that challenge current models of angiopoietin function. Specifically, we demonstrate that Angpt1 is not required in the quiescent mature vasculature but functions as a protective factor, regulating responses to tissue injury and microvascular disease in diabetes.

Results

Generation of mice with a floxed Angpt1 allele. A BAC recombineering approach was used to generate a floxed *Angpt1* allele (Figure 1A), with loxP sites inserted around exon 1. Cre-mediated excision of the floxed allele is predicted to generate a null *Angpt1* allele through frameshift. Correctly targeted ES cell clones were identified by Southern blot analysis with probes outside the region of homology (Figure 1B). The targeting frequency was 16 out of 700 clones (2.3%). After aggregation and breeding of chimeras, heterozygous floxed *Angpt1* mice were bred to mice expressing flp recombinase to remove the Neo cassette.

To confirm that excision of the floxed allele results in a null *Angpt1* allele, *Angpt1*$^{lox/+}$ mice were bred to the pCaggs Cre-driver line that expresses Cre recombinase at the 1-cell embryo stage (11),

Conflict of interest: The authors have declared that no conflict of interest exists.
Citation for this article: *J Clin Invest.* 2011;121(6):2278–2289. doi:10.1172/JCI46322.

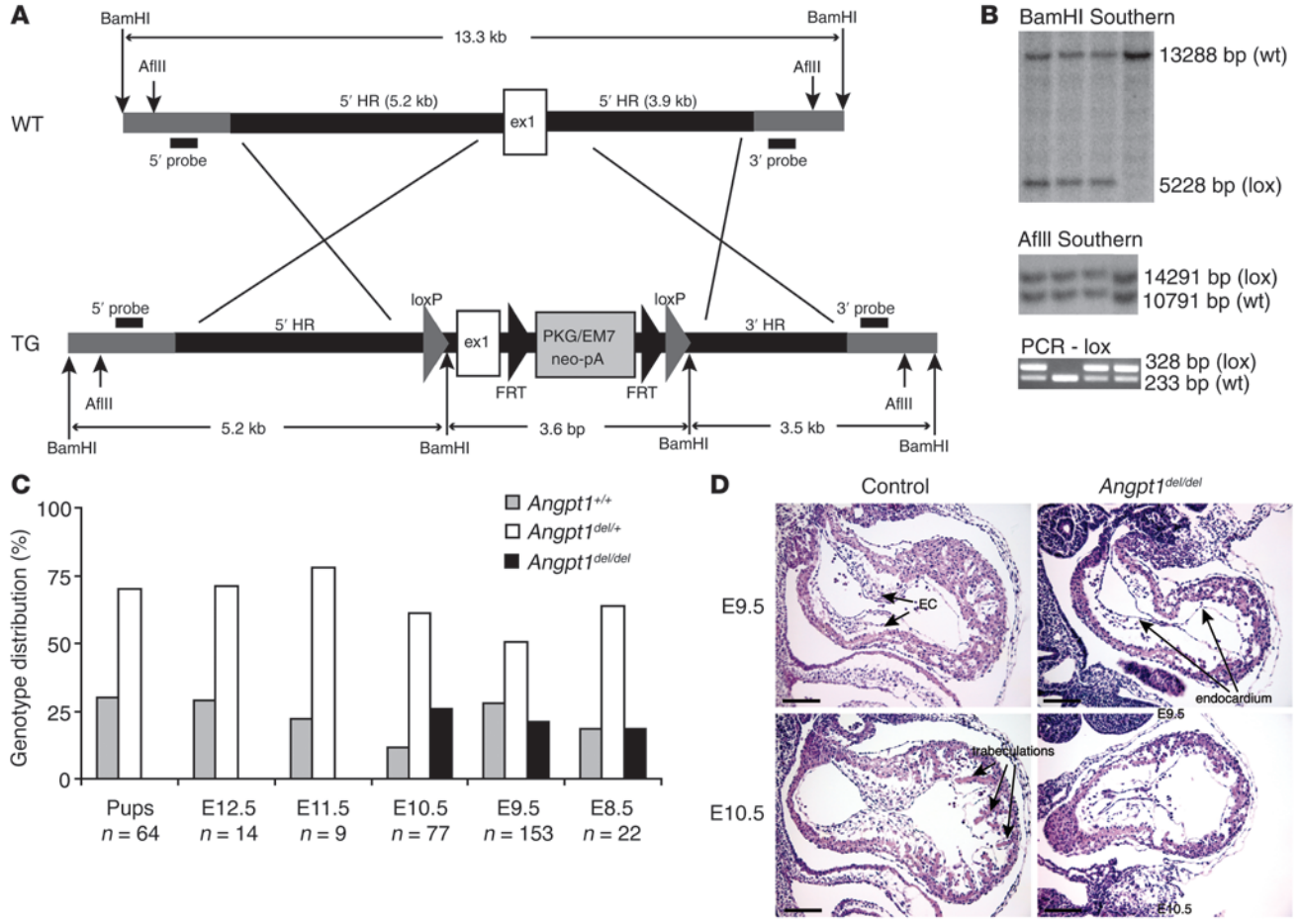

Figure 1
Generation of mice with a floxed *Angpt1* allele. (**A**) Targeting construct for *Angpt1* locus: loxP sites were inserted around exon 1 (ex1). HR, homologous region. (**B**) Correctly targeted ES cell clones were identified using a 3′ probe and a 5′ probe outside of the region of homology, and genotyping of mice was done by PCR. (**C**) Floxed *Angpt1* mice were bred to pCaggs-Cre to generate germline deletion of *Angpt1*, resulting in embryonic lethality in homozygous embryos (*Angpt1*$^{del/del}$ embryos) around E10.5. (**D**) Loss of trabeculations in the heart was observed in E9.5 and E10.5 embryos (scale bar: 100 μm). EC, endocardial cushion.

creating an *Angpt1*^{del} allele. Homozygous deletion (*Angpt1*$^{del/del}$) resulted in embryonic lethality at E9.5 to E12.5 that was identical to that of the conventional knockout and confirmed that the *Angpt1*^{del} allele is functionally a null allele (Figure 1C). *Angpt1*$^{del/del}$ embryos were studied at E9.5 and E10.5. At E9.5, *Angpt1*$^{del/del}$ embryos showed heart defects and loss of heart trabeculations (Figure 1D) identical to those of the conventional knockout (3). Heterozygous embryos showed no phenotype, and a deleted allele was used in breeding to increase Cre-dependent excision.

Angpt1 is critical for cardiac development. The earliest phenotype in the *Angpt1*$^{del/del}$ mice was observed in the heart at E9.5. Specifically, there was marked simplification of the cardiac trabeculation pattern evident at E9.5 and E10.5 (Figure 2, A and B). Optical projection tomography (OPT) was used to study the vasculature of the whole embryos in detail. At E9.5, OPT also showed lack of cardiac trabeculations, but, surprisingly, no other vascular defects were observed. By E10.5, the *Angpt1*$^{del/del}$ embryos were markedly growth restricted (Figure 2C and Figure 3) and exhibited widespread vascular defects, with fusion of vessels with larger diameters and absence of patterning (Figure 3). Despite the vascular defects, *Angpt1*$^{del/del}$ vessels showed coverage of pericytes similar to that of controls (Supplemental Figure 1, A and B; supplemental material available online with this article; doi:10.1172/JCI46322DS1).

Given that the cardiac defects preceded the major vascular defects by an entire day, we wondered whether the extensive vascular defects observed at E10.5, which are reported in the original knockout paper (3), might be a direct consequence of abnormal heart function. To test this, we deleted *Angpt1* specifically in cardiomyocytes using the Nkx2.5–Cre-driver line, *Angpt1*$^{del/^{(heart)}}$ mice. We found that cardiac-specific deletion of *Angpt1* causes embryonic lethality and a phenotype that is virtually identical to that caused by global and conventional *Angpt1* deletion. Quantification of the vascular area of the hindbrain showed a significant increase in vasculature in both *Angpt1*$^{del/del}$ and *Angpt1*$^{del/^{(heart)}}$ embryos compared with that of controls (Figure 3P). Thus, the profound vascular remodeling defects at E10.5 were secondary to the phenotype of cardiac abnormalities and are perhaps due to abnormal blood flow and hemodynamics (Figure 3 and Supplemental Videos 1 and 2). Future studies that allow deletion of

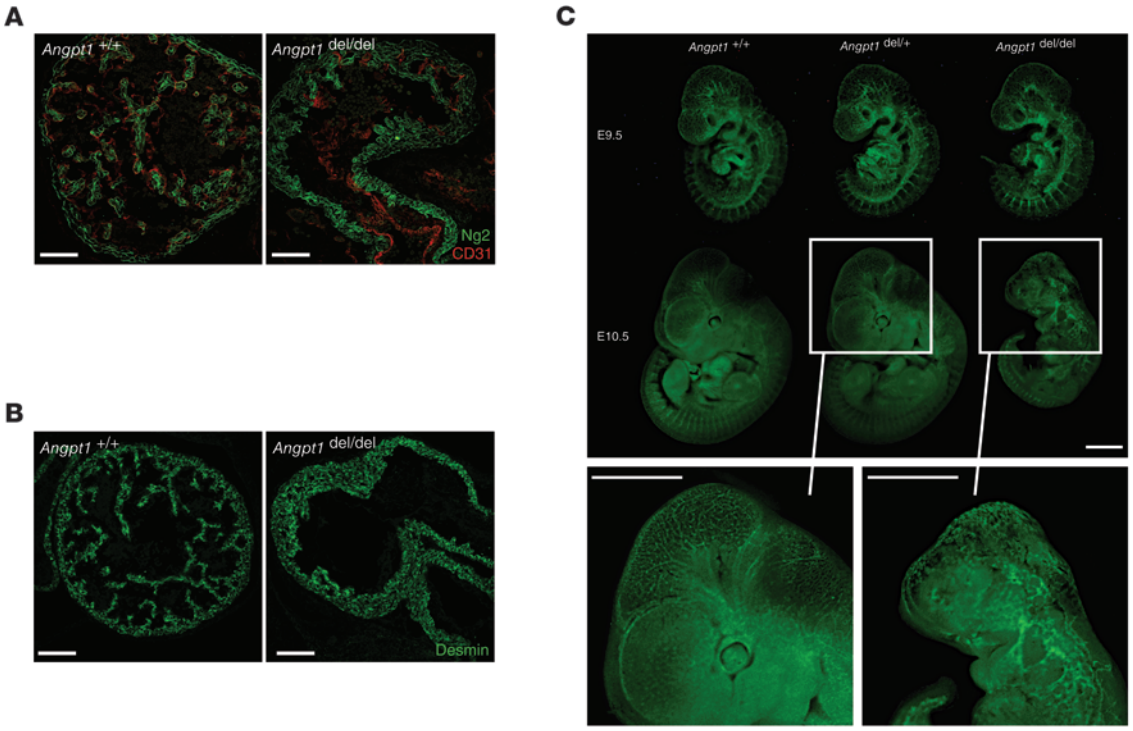

Figure 2
Angpt1 is critical in early vascular development. Simplification of the cardiac trabeculation pattern of E10.5 *Angpt1*$^{del/del}$ embryos as shown by immunohistochemistry for (**A**) Ng2 (scale bar: 100 μm) and (**B**) Desmin (scale bar: 100 μm). (**C**) Dissection microscope photos show that *Angpt1*$^{del/del}$ embryos are markedly growth restricted at E10.5 and have disorganized vasculature as evident in embryos carrying a *Kdr*-GFP transgene reporter (scale bar: 1 mm).

Angpt1 in specific vascular beds but leave cardiac levels intact are required to determine whether there are additional roles for Angpt1 at this early time point.

Angpt1 is required to shape the developing vasculature. To determine whether Angpt1 plays a direct role in vascular development, we used an inducible system to knock out the *Angpt1* allele at each embryonic day. Upon administration of doxycycline (DOX) to the pregnant dam, the ROSA-rtTA/tetO-Cre bitransgenic system was activated to excise the floxed *Angpt1* allele from the entire embryo (Figure 4A). In most cases, an *Angpt1*^{del} allele was used to enhance the degree of excision. PCR and Southern blot analysis of tail genomic DNA confirmed excellent excision of the *Angpt1* gene, i.e., mice only have a deletion band and no floxed band after Cre recombination (Supplemental Figure 2, A and B).

Deletion of *Angpt1* at E10.5, *Angpt1*$^{del/\wedge(E10.5)}$, resulted in embryonic lethality between E17.5 and P0 (Figure 4B). Vascular abnormalities were observed in several organs and were particularly apparent in the liver and kidney, in which vessels were dilated, with veins being more affected than arteries (Figure 4, E–H). In addition, dilated atria were observed in *Angpt1*$^{del/\wedge(E10.5)}$ mice (Figure 4, C and D). Quantification of vessels in the liver showed that there were more vessels and greater vessel area in *Angpt1*$^{del/\wedge(E10.5)}$ mice (Figure 4, V and X). Nonetheless, pericytes were present in equivalent numbers compared to those of controls, as shown by stainings for smooth muscle actin and Pdgfrb (Figure 4, I–N, and Supplemental Figure 1C), and lymphatic vessels appeared normal (Supplemental Figure 3).

In the kidney, dramatic defects were observed in the specialized microvascular beds of the glomeruli, the site of formation of primary urinary filtrate. Many glomerular capillaries exhibited dilated capillary loops and, in some cases, only a single large, open loop (Figure 4, O–T). There are also segments of the glomerular basement membrane (GBM) that were grossly disrupted with numerous folds (Figure 4U). Although mesangial cells were present in *Angpt1*$^{del/\wedge(10.5)}$ embryos, the number appeared reduced in some glomeruli. While the GBM directly beneath the podocytes appeared to be intact, the subendothelial GBM was markedly disorganized and endothelial cell attachment was disrupted (Figure 4U). Structure of podocytes was intact, and they expressed markers of differentiation, such as podocin, similar to wild-type embryos, confirming that this specialized pericyte was also intact (Figure 4, Q and R). Thus, elimination of Angpt1 at E10.5 results in a primary abnormality of the glomerular endothelium and associated matrix production.

Angpt1 is dispensable in the adult vasculature. Deletion of *Angpt1* at any point up to E12.5 had profound consequences, causing death in the perinatal period and the range of structural abnormalities described above. On the other hand, deletion at any time point after E13.5 [*Angpt1*$^{del/\wedge(E13.5)}$] did not affect survival and produced viable, fertile Angpt1-deficient mice, with no overt phenotype (Figure 4B). To ensure that the lack of phenotype was not the result of poor excision, we determined the degree of genomic rearrangement of the allele from multiple tissues using PCR (data not shown). Southern blot analysis showed only a deletion band and no floxed band, confirming close to 100% degree of excision (Supplemental Figure 2A). Real-time PCR demonstrated absence of Ang1 (Supplemental Figure 2, C and D). To determine whether expression of other Tek ligands might be upregulated to compensate for

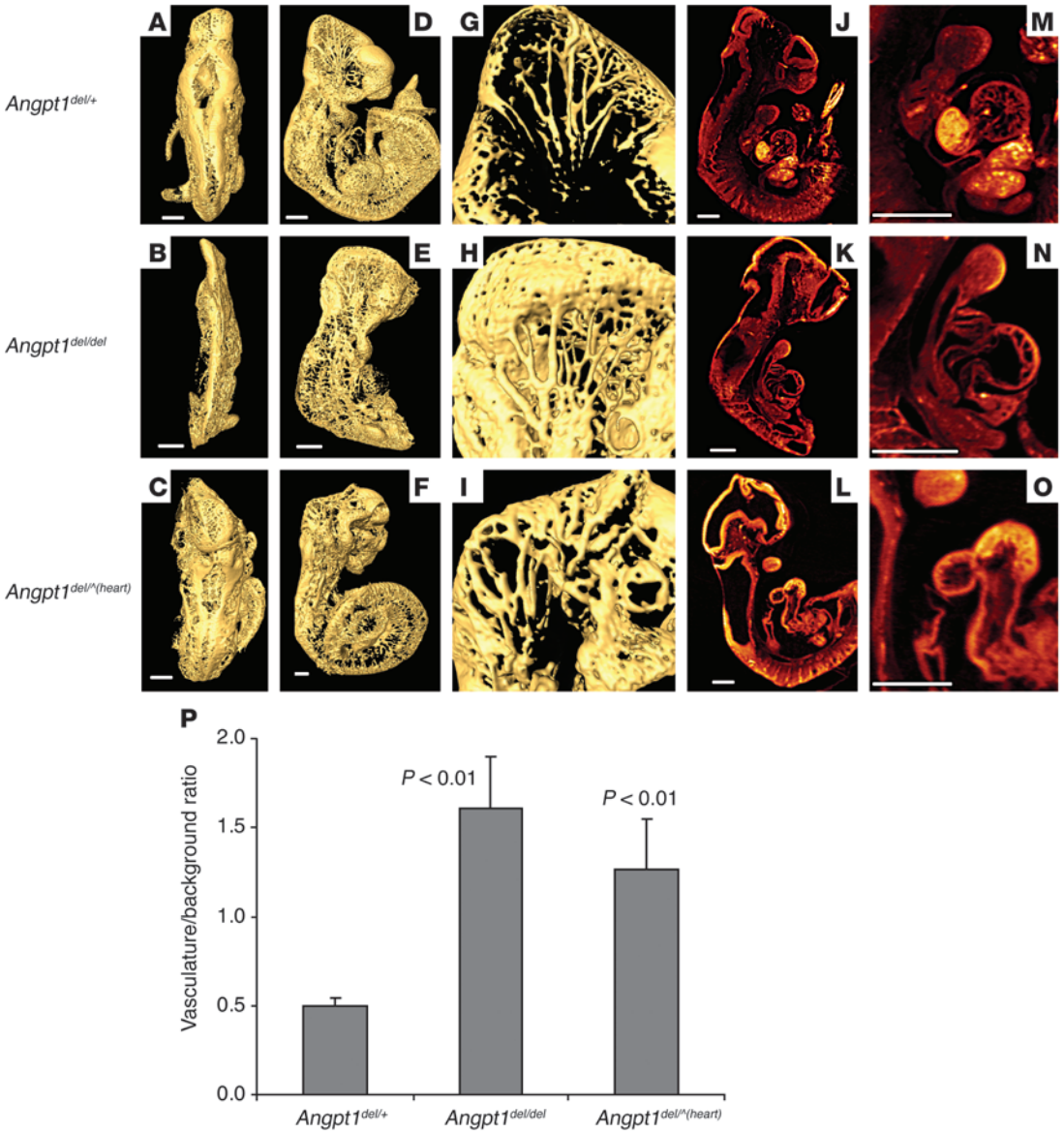

Figure 3

Angpt1 is critical in cardiac development. 3D OPT data showing surface rendering of the vasculature stained with CD31 in E10.5 control, *Angpt1*$^{del/del}$, and *Angpt1*$^{del/\wedge(heart)}$ embryos. Shown are views from (**A**–**C**) behind, (**D**–**F**) the side, and (**G**–**I**) enlargement of the right half of the head. (**J**–**L**) Embryo sections of autofluorescence, (**M**–**O**) with an enlargement of the heart in *Angpt1*$^{del/del}$ and *Angpt1*$^{del/\wedge(heart)}$ embryos. Scale bar: 500 μm. (See also Supplemental Videos 1 and 2.) (**P**) Quantification of hindbrain vascular area shows a significant increase in vasculature in *Angpt1*$^{del/del}$ and *Angpt1*$^{del/\wedge(heart)}$ embryos compared with that of controls.

deletion, we used real-time PCR. No difference was observed in levels of *Angpt2* or *Angpt3* (Supplemental Figure 2, C and D). In addition, we found no difference in the expression of *Tek*, *Tgfb1*, *Vegfa*, *Pdgfb*, and *Pdgfrb* (Supplemental Figure 2, C and D).

Since retinal vascular development occurs from P0 to P5, we examined the retinas of *Angpt1*$^{del/\wedge(E13.5)}$ mice and compared them to those of control littermates. While the retinal neural layers were reduced in number (Supplemental Figure 4A), the retinal vasculature was indistinguishable from that of wild-type mice. Although the number of branch points was more variable in *Angpt1*$^{del/\wedge(E13.5)}$ mutants, the overall number of branch points was not significantly different between the groups (Supplemental Figure 4, B and C). Hyaloid vessels regress by P9 — and again there was no difference between mutant and wild-type mice (n = 2–3; Supplemental Figure 4D). In addition, pericytes were present in equivalent numbers in control and *Angpt1*$^{del/\wedge(E13.5)}$ retinas (Supplemental Figure 1, D and E).

Role of Angpt1 in adult tissues in wound healing and microvascular injury. The viability and absence of a phenotype in mice with *Angpt1* deleted after E13.5 demonstrates that Angpt1 is dispensable in quiescent vasculature. Moreover, these animals provide a useful model for testing the role of Angpt1 in other settings. Previous studies have indicated that Angpt1 may act as a negative regulator of angiogenesis when levels of proangiogenic factors, such as Vegfa,

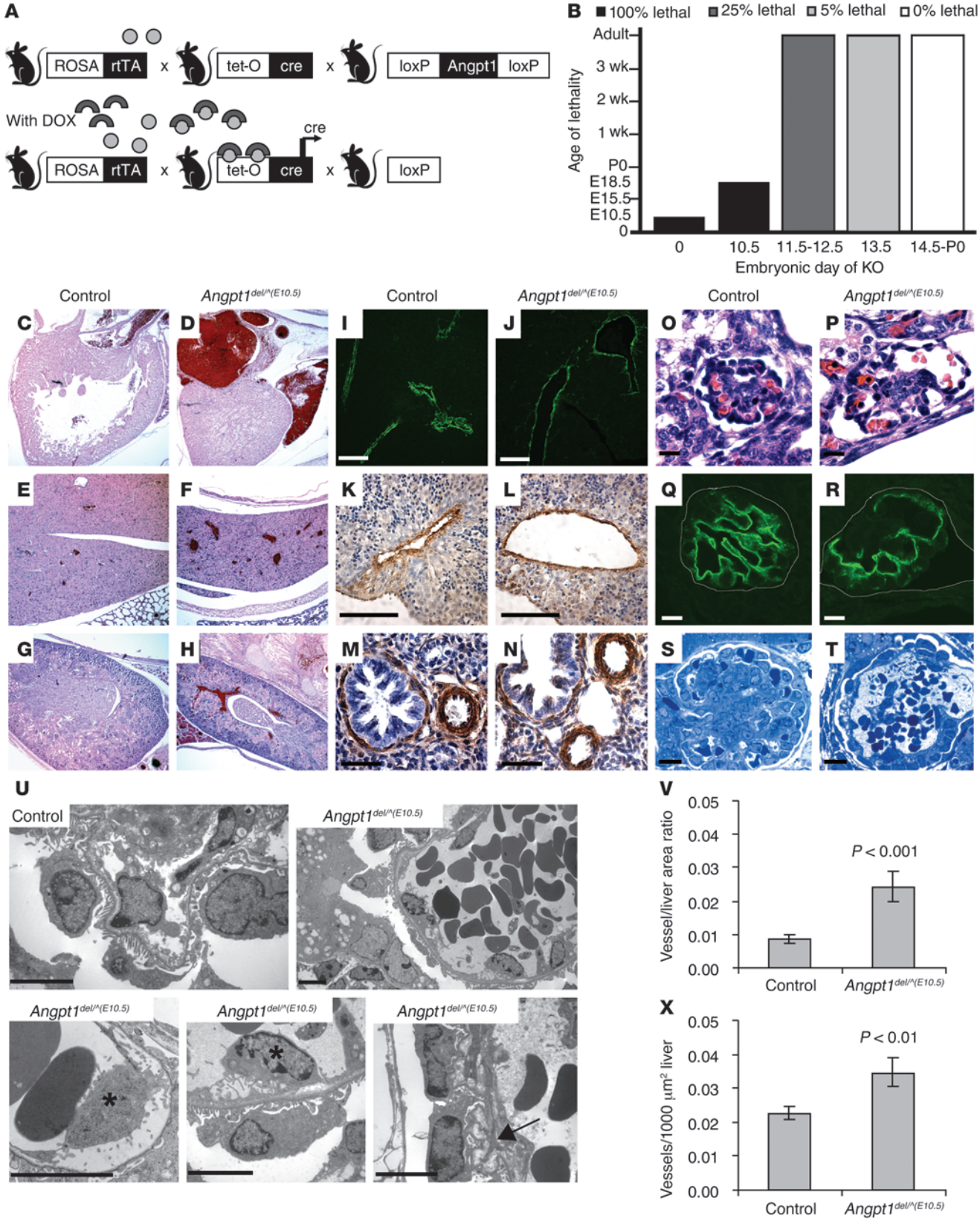
A
ROSA rtTA x tet-O cre x loxP Angpt1 loxP
With DOX
cre
ROSA rtTA x tet-O cre x loxP
B
100% lethal
25% lethal
5% lethal
0% lethal
Age of lethality
Adult
3 wk
2 wk
1 wk
P0
E18.5
E15.5
E10.5
0
0
10.5
11.5-12.5
13.5
14.5-P0
Embryonic day of KO
Control
Angpt1del/^(E10.5)
C
D
I
J
O
P
E
F
K
L
Q
R
G
H
M
N
S
T
U
V
Vessel/liver area ratio
P < 0.001
X
Vessels/1000 μm² liver
P < 0.01

Figure 4
Angpt1 regulates both the number and diameter of developing vessels. (**A**) Breeding strategy to generate inducible whole-body deletion of *Angpt1* [*Angpt1*$^{del/\wedge(DOX)}$ mice] using the DOX-inducible ROSA-rtTA/tetO-Cre bitransgenic system. (**B**) Induction of *Angpt1* knockout at E10.5 [*Angpt1*$^{del/\wedge(E10.5)}$ mice] or earlier results in embryonic lethality. In mice induced with DOX at E10.5, vessels are dilated at P0 (**C** and **D**) in the heart (original magnification, ×50), (**E** and **F**) liver (original magnification, ×50), and (**G** and **H**) kidney (original magnification, ×50). Pericytes/mural cells surround the vessels as shown by α-SMA staining of (**I**–**L**) liver and (**M** and **N**) lung in embryos dissected at E17.5 (See also Supplemental Figure 3). Scale bar: 10 μm (**I** and **J**); 100 μm (**K** and **L**); 50 μm (**M** and **N**). (**V** and **X**) In the same embryos, measurements of vessel number and vessel area in the liver showed a significant increase of both in *Angpt1*$^{del/\wedge(E10.5)}$ embryos compared with those in controls. Deletion of *Angpt1* at E10.5 also resulted in dilated glomerular capillary loops by E17.5, as shown by (**O** and **P**) H&E and (**Q** and **R**) podocin staining (scale bar: 10 μm), and a few glomeruli with only 1 big open capillary loop by P0, as shown by (**S** and **T**) Toluidine Blue staining (scale bar: 10 μm). (**U**) Electron micrographs (scale bar: 5 μm) show a folded GBM (arrow) and detachment of endothelial cells (*).

are elevated (12). To test this in vivo, we used ear punch as a simple model of tissue injury and wound healing in which angiogenesis is stimulated. Using mice with intact capacity for Angpt1 production, we confirmed local upregulation of Vegfa in keratinocytes at the site of wound healing using a *Vegfa*-lacZ mouse (data not shown), consistent with previous reports using real-time PCR (13). We then compared wound healing responses in wild-type mice and mice with induced deletion of *Angpt1* starting at day E13.5–E16.5 [*Angpt1*$^{del/\wedge(E13.5)}$ mice]. The *Angpt1*$^{del/\wedge(E13.5)}$ mice showed an accelerated wound healing response, with almost complete closure by day 60, compared with the minimal response seen in littermate controls. After 60 days, the mean wound area in controls was 3.44 ± 0.30 mm^2, compared with only 0.82 ± 0.14 mm^2 in *Angpt1*$^{del/\wedge(E13.5)}$ mice (Figure 5, A–C). The cartilage and hair follicles were not regenerated in either group, demonstrating that the mechanism of closure is through fibrosis rather than regeneration (Figure 5B). There was a substantial enhancement of angiogenesis and fibrosis in the closed ear tissue in *Angpt1*$^{del/\wedge(E13.5)}$ mice compared with that of controls, as shown by endothelial staining and Masson Trichrome staining of collagen fibers (Figure 5, B and D). Vessels had normal coverage of pericytes (Figure 5E). Thus, after tissue injury, Angpt1 acts to constrain angiogenesis and fibrosis, and, in its absence, these features of wound healing are exaggerated.

Angpt1 protects the glomerular microvasculature in diabetic nephropathy. To examine the role of Angpt1 in a setting of more complex microvascular injury, we used a model of diabetic kidney injury in the mouse. The early phase of diabetic kidney disease is characterized by neoangiogenesis and increased vascular permeability, with leakage of proteins into the urine (albuminuria and proteinuria). Serum levels of both VEGFA and ANGPT2 are increased in diabetics, and there is an elevation of the ANGPT2/ANGPT1 ratio, which is associated with worse cardiovascular and kidney outcomes (9). We confirmed the upregulation of *Vegfa*, *Angpt2*, and *Tgfb1* in glomerular cell fractions in the streptozotocin (STZ) model of diabetes by using a kinase insert domain protein receptor–GFP (*Kdr*-GFP) (*Kdr* is also known as *Flk1*) transgenic mouse and FACS (Figure 6A).

To examine the role of Angpt1 in diabetes, controls and mice with *Angpt1* deletion starting between E16.5 and P0 [*Angpt1*$^{del/\wedge(E16.5)}$ mice] were used. At the age of 4–6 weeks, they were given injections of the β cell toxin STZ to induce diabetes and were then monitored for up to 20 weeks. This regimen typically causes robust hyperglycemia but has only modest effects on kidney structure and function in wild-type mice (14), which was the case for control mice in our study. By contrast, 20% of the diabetic *Angpt1*$^{del/\wedge(E16.5)}$ mice died before the end of the study, whereas all control mice survived ($P < 0.05$, Figure 6B). The surviving diabetic *Angpt1*$^{del/\wedge(E16.5)}$ mice have impaired function of the glomerular filtration barrier (GFB), manifested by significant albuminuria, with urinary albumin/creatinine ratios of 0.25 (+0.08, –0.06) mg/mg in diabetic *Angpt1*$^{del/\wedge(E16.5)}$ mice compared with ratios of 0.06 ± 0.01 mg/mg in diabetic controls (Figure 6C). On histopathological examination of the kidney, diabetic controls had minimal abnormalities confined to mild mesangial expansion. However, there were marked changes in glomerular histology in the diabetic *Angpt1*$^{del/\wedge(E16.5)}$ mice, with dramatic mesangial matrix expansion and glomerulosclerosis (Figure 6D); similar pathological features can be seen in humans with advanced diabetic nephropathy. Such changes were never seen in diabetic controls or nondiabetic groups and have rarely been reported in other studies of diabetic kidney injury in mice (14, 15). Despite the differences in glomerular pathology, the extent of hyperglycemia achieved was not different between the groups, as reflected by the similar levels of glycosylated hemoglobin (HbA1c) at the end of the study [0.088% ± 0.003% vs. 0.090% ± 0.003% for diabetic controls and diabetic *Angpt1*$^{del/\wedge(E16.5)}$ mice, respectively] (Figure 6E). F4/80-positive macrophage infiltration was increased in kidneys from diabetic compared with nondiabetic mice; however, there was no difference between controls and *Angpt1*$^{del/\wedge(E16.5)}$ mice in diabetic or nondiabetic conditions (data not shown).

To define the key cellular sources of Angpt1 that protect the glomerulus in diabetes, we generated separate lines of mice with *Angpt1* deleted specifically from podocytes or mesangial cells [*Angpt1*$^{del/\wedge(glom)}$ mice] using podocyte- and mesangial-expressed Cre drivers (16, 17). After STZ treatment, only compound mutants (i.e., both *Nphs1*-Cre and *Pdgfrb*-Cre mice) showed a similar degree of accelerated glomerular damage as the global diabetic *Angpt1*$^{del/\wedge(E16.5)}$ mice, indicating that production of Angpt1 by each of these glomerular cell populations provides protection against microvascular injury in diabetes (Figure 6D). Thus, local production of Angpt1 by glomerular cell populations, including the podocyte and mesangial cell, provides significant protection against diabetic kidney injury.

Discussion

Developmental and pathologic angiogenesis are complex processes under exquisite control. VEGF and angiopoietin are 2 major vascular tyrosine kinase signaling pathways controlling angiogenesis. Whereas VEGF is established as a major regulator of blood vessel biology in the adult, much less is known about the requirement of the ANGPT/TEK system, especially in mature vessels. An increase in the ratio of circulating ANGPT2/ANGPT1 has been suggested to be a biomarker for increased morbidity and mortality in a variety of clinical syndromes characterized by endothelial dysfunction that include diabetes (9), indicating a potential role for dysregulated ANGPT/TEK signaling in pathological conditions. As conventional *Angpt1* knockout mice die at midgestation due to cardiovascular defects, we generated a conditional *Angpt1* allele that allows deletion of *Angpt1* at specific embryonic, postnatal, and adult time-points and in specific cell compartments in order to define the physiological functions of Angpt1/Tek signaling.

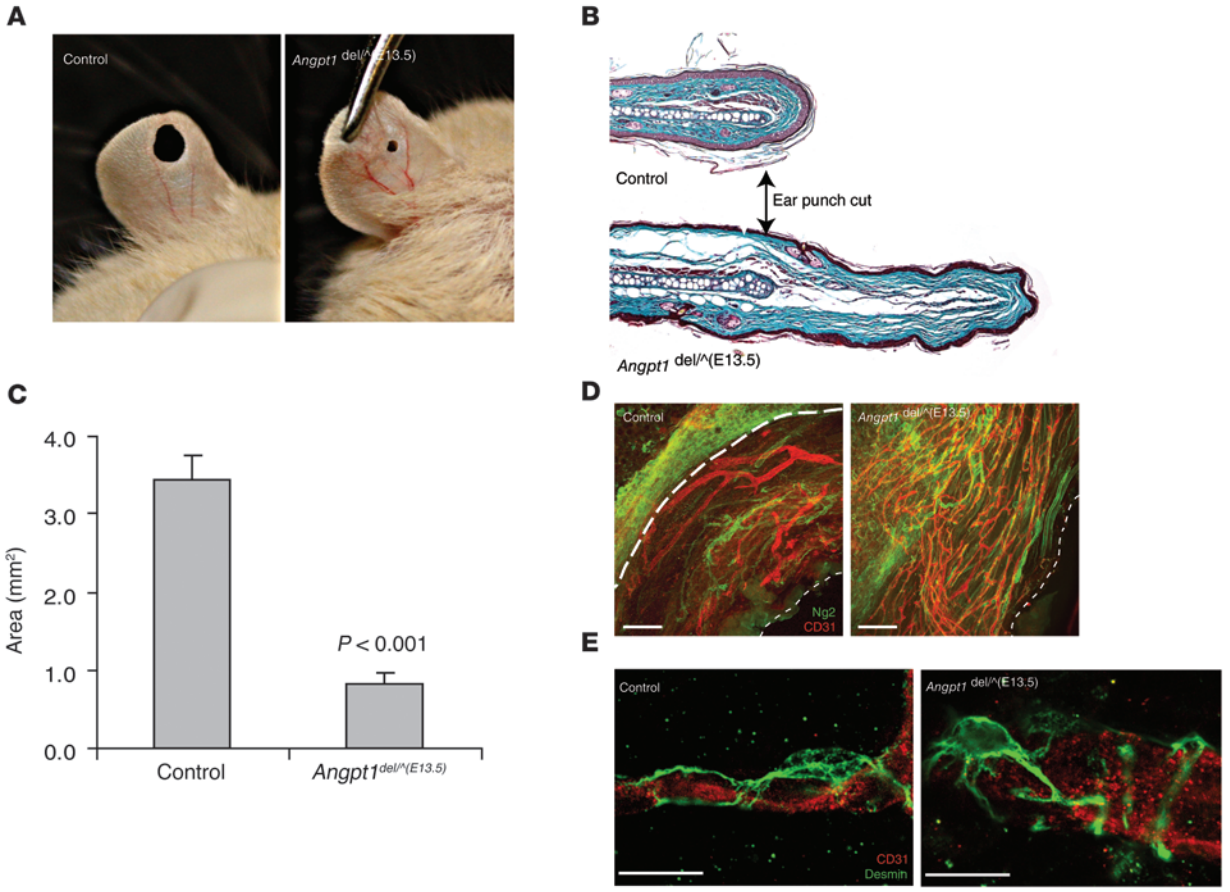

Figure 5
Angpt1 regulates tissue response in wound healing. (**A**) Wound closure in ear punch wounds is increased in *Angpt1*$^{del/\wedge(E13.5)}$ mice. (**B**) Cross sections of one of the sides of the ear punch show the cut of cartilage and the larger closed zone in *Angpt1*$^{del/\wedge(E13.5)}$ mice (Masson Trichrome) (original magnification, ×100). (**C**) Quantification (mean ± SEM) of the punch area after 60 days shows a significant decrease in open area in the *Angpt1*$^{del/\wedge(E13.5)}$ mice. (**D**) Z-stacks of flat mounted ears stained for CD31 (red, endothelium) and Ng2 (green, pericytes) show increased angiogenesis in the closed zone of *Angpt1*$^{del/\wedge(E13.5)}$ mice compared with that of controls (scale bar: 100 μm). Z-stacks are composed of 8 images every 3 μm. The thick line (only in control) is the start of the closed zone (cut), and the thin line is the edge of the closed zone. (**E**) The close up of vessels in the healed area shows normal pericyte coverage (Desmin, green) of vessels (scale bar: 10 μm).

Using an early embryonic global Cre deleter strain (pCaggs-Cre) to generate a null *Angpt1* allele (*Angpt1*^{del}), we confirmed previous studies showing that mice homozygous for this null allele (*Angpt1*$^{del/del}$ mice) die between E10.5 and E12.5. OPT imaging of these *Angpt1*$^{del/del}$ embryos revealed that the earliest detectible defect, seen at E9.5, was loss of trabeculations in the heart, while the remainder of the vascular system appeared normal. Within 24 hours, the *Angpt1*$^{del/del}$ embryos became markedly growth restricted, with generalized disorganization of blood vessels. Given the primary and profound cardiac defect, we wondered whether the subsequent vascular defects observed at E10.5 resulted from cardiac dysfunction and reduced blood flow rather than a primary effect of Angpt1 on the vasculature. Indeed, when *Angpt1* is excised from cardiomyocytes alone [*Angpt1*$^{del/\wedge(heart)}$], using the nkx-2.5 Cre-driver line, the vascular defects reported in the conventional knockout are recapitulated, indicating their dependence on the cardiac defect (3).

While its earliest role is in the heart, Angpt1 also regulates later phases of vascular development, which could not be studied in the conventional knockout. In this regard, deletion of *Angpt1* between E10.5 and E12.5 causes severe vascular defects in all organs and lethality. When *Angpt1* is deleted during this period, we find a greater overall number of vessels, increased vessel diameters, and a disorganized vascular network. One of the key roles suggested for *Angpt1* is in development and recruitment of pericytes, cells that serve as important vascular support structures. Nonetheless, we find that the loss of Angpt1 does not affect either pericyte number or vascular mural cell recruitment. Specifically, using several markers for pericytes, including Pdgfrb, Ng2, Desmin, and α-smooth muscle actin, and examining a number of tissues, we find normal coverage of vessels by pericytes, across a range of time points of *Angpt1* deletion. For example, the number and structure of glomerular pericytes, known as podocytes, were completely normal in *Angpt1* mutant mice. Likewise, vascular smooth muscle cells were also present in normal pattern and quantity. By contrast, there are overt defects in capillary basement membranes in affected vascular beds, such as the renal glomerulus, when *Angpt1* is deleted at E10.5, suggesting that impaired Tek signaling in endothelial cells may primarily cause defects in production of extracellular matrix.

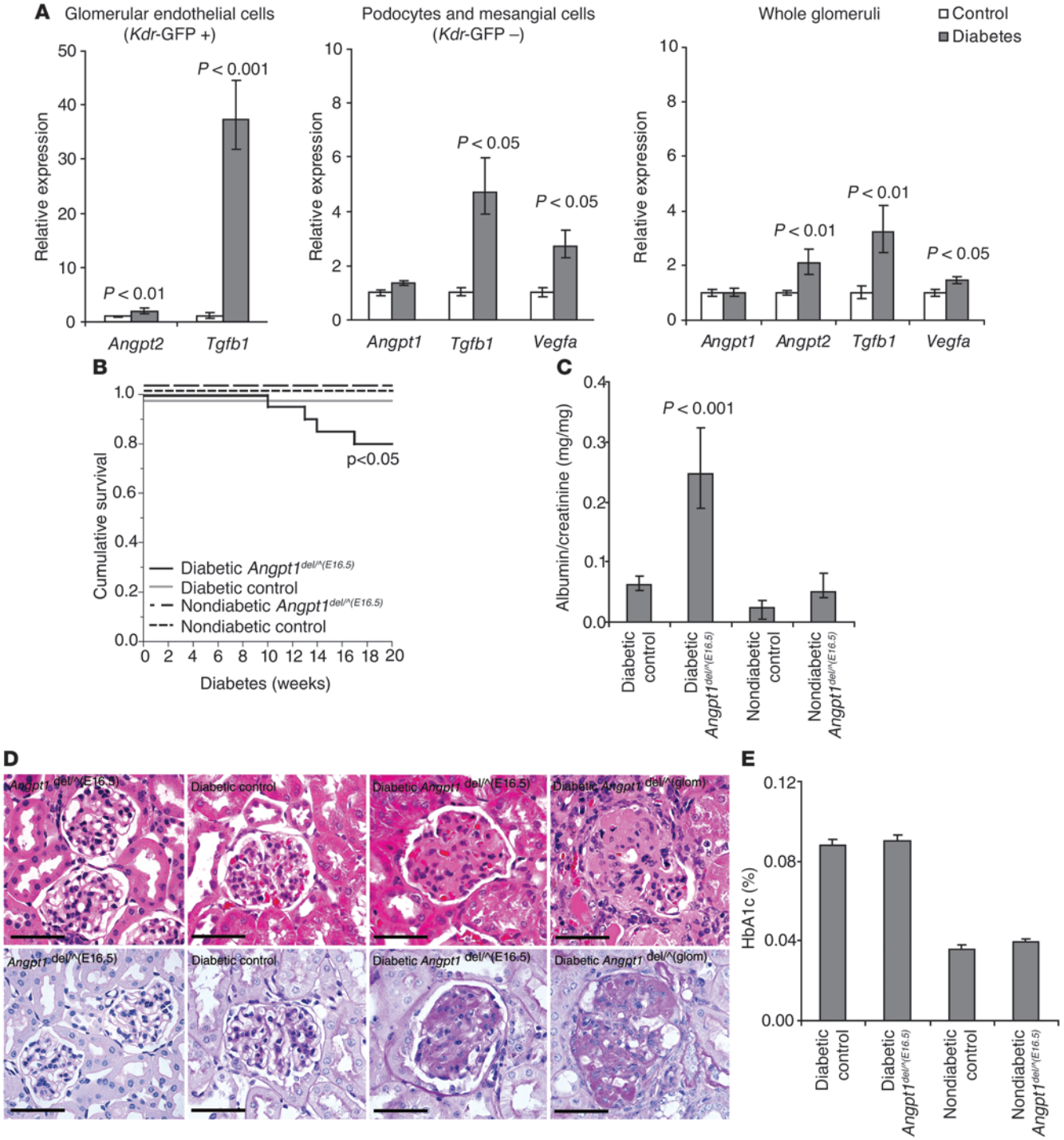

Figure 6

Angpt1 protects the glomerular vasculature in diabetic nephropathy. (**A**) Expression of *Angpt1*, *Angpt2*, *Tgfb1*, and *Vegfa* in whole glomeruli or cell fractions sorted by FACS from diabetic and nondiabetic mice carrying a *Kdr*-GFP transgene reporter (mean ± SEM). FACS cells from glomeruli are endothelial cells in the GFP-positive fraction (*Kdr*-GFP +) and mainly podocytes and mesangial cells in the GFP-negative fraction (*Kdr*-GFP –). (**B**) *Angpt1*$^{del/\wedge(E16.5)}$ mice (induced between E16.5 and P0) made diabetic show a significant decrease in survival. (**C**) After 20 weeks of diabetes, *Angpt1*$^{del/\wedge(E16.5)}$ mice have a significantly higher urinary albumin/creatinine ratio compared with that of controls and nondiabetic groups. (**D**) Histology shows an increase in mesangial matrix expansion and sclerosis in diabetic *Angpt1*$^{del/\wedge(E16.5)}$ mice and diabetic *Angpt1*$^{del/\wedge(glom)}$ mice compared with that of diabetic controls (H&E, top panel; PAS bottom panel) (scale bar: 50 μm). (**E**) HbA1C in controls and *Angpt1*$^{del/\wedge(E16.5)}$ mice is comparable in nondiabetic mice and after 20 weeks of diabetes.

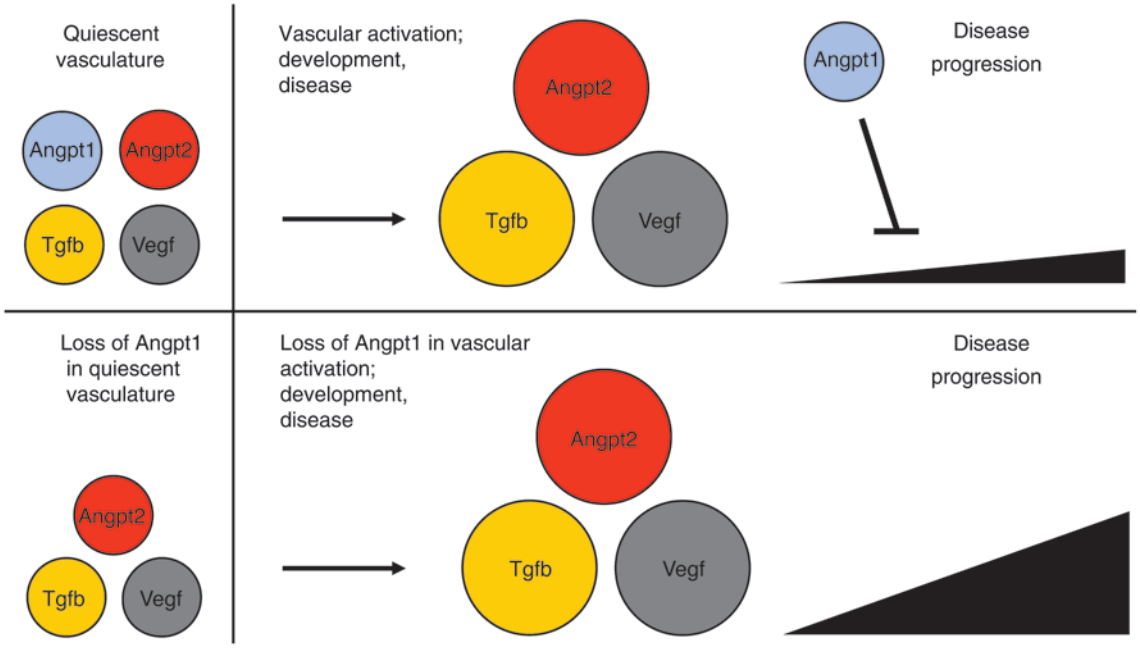

Figure 7
Model for Angpt1 function during vascular activation. Schematic model showing the importance of Angpt1 as an inhibitor of disease progression in the case of vascular activation that occurs in development or disease. In the absence of Angpt1, Angpt2, Vegfa, and Tgfb, actions are unopposed, resulting in more aggressive injury in disease or a larger number and diameter of vessels in development.

While our studies document these key roles for Angpt1 in development, its actions are apparently dispensable in adulthood. Specifically, we found that a deletion of *Angpt1* after E13.5 does not cause any overt phenotypes; the animals were viable, fertile, and appear healthy. This is in stark contrast to Vegfa, where deletion causes severe phenotypes during development and in mature animals (18, 19). Numerous studies have suggested that Angpt1/Tek signaling is required to maintain mature "leak-free" vessels (20, 21), and overexpression of Angpt1 was shown to promote generation of mature vessels resistant to leak (22). In contrast, our results show that endogenous Angpt1 is not required to maintain vascular integrity or reduce permeability in mature, quiescent vascular beds. Focusing on the GFB and the blood brain barrier, networks that have been analyzed in previous studies (23, 24), we were unable to detect any enhanced vascular permeability in mutant mice with deletion of *Angpt1* from E13.5 onward (data not shown). These results suggest that in mature, quiescent vessels, Angpt1 production is not required to regulate permeability.

Whereas ongoing Vegfa/Vegfr2 signaling is required to maintain endothelial cell survival and differentiation in specific vascular beds such as the renal glomerulus (25) and liver (S.E. Quaggin, unpublished observations), we propose that Angpt1 has a different but equally important role. We posit that Angpt1 functions as a "brake" to balance and modulate angiogenic activity, allowing formation of the proper number and size of vessels. This function is evident in the presence of a proangiogenic stimulus, such as during development and certain pathologic states. In these settings, the levels of Vegfa and Angpt2 are elevated, promoting new vessel growth. However, in the absence of proangiogenic stimuli following vessel maturation, Angpt1 is not required (Figure 7). In essence, we propose that Angpt1 functions like the brakes in a car — which are required to stop a moving vehicle but are redundant in a stationary one.

To test this hypothesis, we assessed responses of *Angpt1* mutant mice to clinically relevant states characterized by enhanced angiogenesis. For example, after tissue injury, healing occurs through an initial phase of angiogenesis followed by tissue fibrosis or regeneration. In both instances, the early phase is associated with enhanced expression of Angpt2 and Vegfa expression locally around the wound; Vegfa is upregulated in keratinocytes, whereas Angpt2 is increased in endothelial cells (13, 26). Accordingly, we induced a controlled tissue injury using an ear punch (27). In $Angpt1^{del/\wedge(E13.5)}$ mice, ear closure is rapid and significantly more robust than that in wild-type littermates. Moreover, wound closure is associated with aggressive fibrosis following the active angiogenic phase. Similarly, angiogenesis that occurs in transgenic mice engineered to overexpress *Angpt2* and *Vegfa* in the myocardium is also accompanied by an aggressive fibrotic response, and this response is inhibited by coexpression of *Angpt1* (12). One of the factors implicated in promoting fibrotic responses is Tgfb, which also modulates angiogenesis (28). Thus, Angpt1 might oppose Tgfb-mediated fibrosis, along with its effects on Vegfa/Angpt2-mediated angiogenesis.

Cho et al. also showed an increase in wound closure after treatment with cartilage oligomeric matrix protein–Angpt1 (COMP-Angpt1) and attributed this to increased angiogenesis, lymphangiogenesis, and blood flow (29). How can loss of Angpt1 and exaggerated levels of COMP-Angpt1 produce apparently similar phenotypes? COMP-Angpt1 is more potent than native Angpt1 in phosphorylating Tek and also induces larger vessels and increased blood flow (30), mimicking the activating mutation of TEK seen in inherited venous malformations (31). Apelin, a Tek-induced ligand for APJ, has been shown to regulate vessel size and increase endothelial cell proliferation together with Vegfa (32). While activation of Tek enhances angiogenesis, inhibition of Tek through upregulation of Angpt2 also augments Vegfa-mediated

angiogenic responses (12, 33), whereas the presence of Angpt1 blunts this angiogenic response (12). Thus both gain- and loss-of-function mutations in Angpt/Tek signaling could cause similar angiogenic phenotypes but through different mechanisms. On the other hand, enhanced fibrosis is a major feature of wounds in *Angpt1*$^{del/\wedge(E13.5)}$ mice but was not reported in the COMP-Angpt1 study, suggesting at least one key difference between these wound closure phenotypes. Furthermore, the exaggerated fibrotic response in *Angpt1*$^{del/\wedge(E13.5)}$ mice is consistent with observations that COMP-Angpt1 attenuates renal fibrosis in a UUO model (34). Despite these differences, our studies suggest that inhibition of Angpt1 might be used to enhance wound closure, perhaps in different circumstances than COMP-Angpt1.

Diabetic nephropathy is the leading cause of end-stage kidney disease in North America, and dysregulated angiogenesis has been suggested to be a critical component of its pathogenesis (35). In this regard, a role for altered production of VEGFA has been emphasized (9, 35). Thus, we induced diabetes in *Angpt1*$^{del/\wedge(E16.5)}$ mice with STZ and characterized the resultant kidney injury. Typically, STZ-induced diabetes is associated with only mild functional and pathological abnormalities in mice (14), and this was the case in our control group. On the other hand, loss of Angpt1 in diabetes causes aggressive nephropathy characterized by increased glomerular permeability, accelerated fibrosis, and enhanced mortality. This acceleration of diabetic kidney injury is among the most severe of any reported mouse model of diabetic nephropathy (14, 15). We further demonstrate that *Vegfa*, *Angpt2*, and *Tgfb* levels were increased in the glomeruli of diabetic mice; *Vegfa* expression was upregulated in podocytes, whereas *Angpt2* expression was increased in the adjacent glomerular endothelial cells, and *Tgfb1* was increased in both fractions. Based on our hypothetical model described above, we suggest that the increase in glomerular levels of Vegfa, Angpt2, and Tgfb1 favors the development of glomerular injury, and the absence of the counterbalancing actions of Angpt1 results in an aggressive form of nephropathy. While most work to date in diabetes and angiogenesis has focused on VEGF (9, 35), our results emphasize an important role for the Angpt/Tek system.

Despite the availability of VEGFA inhibitors for clinical use, their utility in the treatment of diabetic nephropathy will likely be limited due to ongoing requirement for and exquisite sensitivity of the healthy glomerular endothelium to alterations in VEGFA. In this regard, both upregulation and downregulation of *Vegfa* have profound effects on glomerular function in transgenic models (18, 19, 36). Furthermore, glomerular injury has emerged as a major toxicity in cancer patients treated with VEGF inhibitors (19). However, since Angpt/Tek signaling is not required in the normal glomerulus or vasculature, this pathway may be a more appealing therapeutic target. This possibility is further supported by promising renoprotective results of COMP-Angpt1 administration in the db/db model of type 2 diabetes in mice (37).

In summary, the major findings of this study reveal that Angpt1 is essential for vascular development but is dispensable in quiescent vessels. In addition, we found that the major defects observed in the original reports of *Angpt1*-null mice can be explained by a primary cardiac defect. While Angpt1 plays additional roles in the developing vasculature to generate appropriately sized vessels, this does not involve regulation of pericyte recruitment or smooth muscle cell investment. Finally, we demonstrate that Angpt1 is required to protect the vasculature in situations of enhanced angiogenesis and fibrogenesis. Accordingly, we propose that Angpt1 functions to balance enhanced Vegfa, Angpt2, and Tgfb levels, limiting the angio-fibrogenic response (Figure 7). In contrast to the Vegf system, in which manipulation at any time point during development or in the adult results in profound phenotypes, the Angpt/Tek system appears to be a promising therapeutic target, since manipulation may modulate pathologic vessel growth without affecting the normal vascular functions.

Methods

Mice and breeding. All experiments were approved by the Animal Care Committee of Mount Sinai Hospital (Toronto, Ontario, Canada) and were conducted in accordance with guidelines established by the Canadian Council on Animal Care.

To generate a conditional allele for the *Angpt1* gene, loxP sites were inserted around exon 1 (Figure 1A). The construct was built according to the published protocol for BAC homologous recombination (38). The construct was linearized, precipitated, and electroporated into R1 (129SV strain) ES cells as described previously (39) and selected using both positive and negative selection. Homologous recombination was confirmed by Southern blot analysis using 2 probes outside of the region of homology (Figure 1B). In total, 700 ES cell clones were picked, and 16 clones were identified as correctly targeted. After expansion of cells, 2 clones were chosen for aggregation with embryos as described previously (39). Strong chimeras were obtained and bred to ICR wild-type albino mice to determine germline transmission. Mice positive for the floxed allele were then bred to mice expressing flp recombinase (40) to remove the Neo cassette and to mice expressing pCaggs Cre (11) to generate a germline deletion of *Angpt1* (*Angpt1*^{del} mice). Nkx2.5-Cre transgenic mice were used to generate mice lacking *Angpt1* expression in cardiomyocytes [*Angpt1*$^{del/\wedge(heart)}$ mice]. The ROSA-rtTA/tetO-Cre transgenic system, as described previously (25), was used to generate inducible whole-body knockout of *Angpt1*, *Angpt1*$^{del/\wedge(DOX)}$ mice, upon administration of DOX in the drinking water (0.2 g DOX, 5 g sucrose per 100 ml water). Mice were kept on DOX for 3 weeks. *Angpt1*$^{del/\wedge(DOX)}$ mice were bred to have 1 allele each of *Angpt1*^{lox}, *Angpt1*^{del}, ROSA-rtTA, and tetO-Cre. Controls were mice lacking 1 of the alleles (heterozygous mice had no phenotype). In addition, *Nphs1*-Cre or *Nphs2*-Cre transgenics (16), together with *Pdgfrb*-Cre mice (17), were used to generate deletion of *Angpt1* in the renal glomerulus [*Angpt1*$^{del/\wedge(glom)}$ mice]. The *Pdgfrb-Cre* mouse was provided by R.H. Adams (Max Planck Institute for Molecular Biomedicine, Münster, Germany). The following genotyping primers were used: *Angpt1*^{lox} (forward, 5-CAATGCCAGAGGTTCTTGTGAA; reverse, 5-TCAAAGCAACATATCATGTGCA; wild type 233-bp product, floxed 328-bp product) and *Angpt1*^{del} (forward, 5-CAATGCCAGAGGTTCTTGTGAA; reverse, 5-TGTGAGCAAAACCCCTTTC; 431-bp product).

3D OPT and immunohistochemistry. Control, *Angpt1*$^{del/del}$, and *Angpt1*$^{del/\wedge(heart)}$ embryos dissected at E9.5 and E10.5 were processed for 3D OPT, which has been described previously (41). Briefly, embryos were fixed in 4% PFA for 4 hours at 4°C and washed in PBS. Catalase was inactivated by incubation in 50 mM sodium azide, followed by endogenous peroxidase activity quenching in 3% H_2O_2. Nonspecific antibody binding was blocked by incubation in 1% heat-inactivated FCS and 1% normal goat serum. Embryos were then stained overnight with 5 μg/ml anti-CD31 antibody (Mec13.3 clone, BD Pharmingen). Primary antibody was detected by overnight staining with HRP-conjugated anti-rat secondary antibody, followed by incubation with tyramide-Cy3 reagent (1:50; Perkin Elmer) for 1 hour. Embryos were mounted in 1% low-melting-point agarose and imaged using a Leica MZFLIII stereozoom microscope and a Retiga Exi CCD camera (see ref. 41 for details). In order to determine the extent of vasculature present in the hindbrains of the embryos, surface-rendered images of each individual embryo were digitally sliced along the sagittal midline of their respective

heads, and each of the halves of their brains were examined over several threshold values. Snapshots of the hindbrains were taken, converted into a black (background) and white (vasculature) binary images, and the ratio of the vasculature pixels to background pixels was calculated (n = 4–8). The value shown for the individual embryo genotypes is agreeable to within 10% across many threshold values.

The same staining protocol was used for flat mount retinas. Several ×20 confocal images (Nikon C1si) were stitched together to create images of the whole retinal primary capillary plexus. The number of branch points was calculated between 2 arteries from P5 retinas from control and *Angpt1*$^{del/\wedge(E13.5)}$ mice (n = 2–3).

Additional primary antibodies used for standard immunohistochemistry of ears, frozen sections, and paraffin-embedded sections after antigen retrieval include rabbit anti–α-smooth muscle actin antibody (ab5694, Abcam), rabbit anti-Desmin antibody (ab15200, Abcam), rabbit anti-Ng2 antibody (AB5320, Millipore), and rabbit anti-Podocin antibody (P0372, Sigma-Aldrich), goat anti-Lyve1 antibody (AF2125, R&D Systems), and rabbit anti-Pdgfrb antibody (ab32570, Abcam). In the case of paraffin-embedded sections, endothelium was stained with Texas Red–conjugated *Lycopersicon esculentum* (Tomato) Lectin (TL-1176, Vector Laboratories).

Ear punch experiments. Controls (n = 10) and *Angpt1*$^{del/\wedge(E13.5)}$ (n = 9) mice (induced with DOX from E13.5 to E16.5) were used for the experiments. A hole was punched in the center of the cartilaginous part of the left ear, using a 2.05-mm diameter metal ear punch (Harvard Apparatus) as described previously (27). Photographs of wounds were taken in the presence of a scaled ruler after 60 days. To quantify the wound area, digital pictures were taken and analyzed using the UTHSCSA Image Tool 3.0 software (http://ddsdx.uthscsa.edu/dig/download.html).

Diabetes. Male control mice (n = 17) and *Angpt1*$^{del/\wedge(E16.5)}$ mice (n = 20) (induced with DOX starting between E16.5 and P0) were made diabetic by i.p. injection of 50 mg/kg STZ (Sigma-Aldrich) dissolved in Na-Citrate buffer for 5 consecutive days (using a Animal Models of Diabetic Complications Consortium protocol; www.AMDCC.org). Mice with blood glucose of more than 15 mmol/l were included in the study. Glycosylated hemoglobin (HbA1c) was measured in blood from heart puncture at the end of the study. Nondiabetic controls (n = 15) and *Angpt1*$^{del/\wedge(E16.5)}$ mice (n = 8) were also included in the study. In addition, mice with *Angpt1* deleted specifically from podocytes (Nphs1-Cre) and mesangial cells (Pdgfrb-Cre) were used [*Angpt1*$^{del/\wedge(glom)}$ mice]. Urine albumin/creatinine ratios were calculated by measuring albumin (Albuwell M ELISA, Exocell Inc.) and creatinine (Jaffe method, KGE005, R&D Systems) in spot urine.

To investigate expression of genes in different cell types of the glomerulus, we induced diabetes in transgenic mice carrying an endothelial linage marker (*Kdr*-GFP mice) (42). Glomeruli were isolated by sieving, and a single cell suspension was obtained by enzymatic digestion (1 mg/ml collagenase A, 1 mg/ml collagenase IV, 1 mg/ml collagenase V, 1 mM EDTA, 25 mM HEPES in HBSS) at 37°C for 1 hour on shaker. After washing and resuspension, cells were sorted into positive and negative fractions for *Kdr*-GFP using FACS (BD FACSAria) with low-sheet pressure (20 psi).

Real-time PCR. TRIzol was used to prepare mRNA from tissue and cells according to the manufacturer's instructions (Invitrogen) and reverse transcribed for real-time PCR using a cDNA synthesis kit (iScript, Bio-Rad). Real-time PCR was performed using iTaq SYBR Green Supermix (Bio-Rad) with appropriate primers in an ABI Prism 7900 Sequence Detection System (Applied Biosystems). Gene expression was calculated and expressed relative to a housekeeping gene (*Hprt*) using the $\Delta\Delta C_T$-method (Applied Biosystems). The following primers (Sigma-Aldrich) were used: *Angpt1* (forward, 5-GGGGGAGGTTGGACAGTAA; reverse, 5-CATCAGCTCAATCCTCAGC), *Angpt2* (forward, 5-GATCTTCCTC-CAGCCCCTAC; reverse, 5-TTTGTGCTGCTGTCTGGTTC), *Hprt* (forward, 5-GGCTATAAGTTCTTTGCTGACCTG; reverse, 5-AACTTTTAT-GTCCCCCGTTGA, *Angpt3* (forward, 5-GAGACGTAATGCCACCACCT; reverse, 5-GAGTGTCCAGCTTCCTTTGC), *Tek* (forward, 5-TGGAGT-CAGCTTGCTCCTTT; reverse, 5-ACCTCCAGTGGATCTTGGTG), *Vegfa* (forward, 5-CAGGCTGCTGTAACGATGAA; reverse, 5-CTATGTGCTG-GCTTTGGTGA), *Tgfb1* (forward, 5-GCTGCGCTTGCAGAGATTAAA; reverse, 5-TTGCTGTACTGTGTGTCCAG), *Pdgfb* (forward, 5-ACTC-CATCCGCTCCTTTGAT; reverse, 5-GTCTTGCACTCGGCGATTA), *Pdgfrb* (forward, 5-CAACCGTACCTTGGGTGACT; reverse, 5-GAGA-GCTGGACCTCATCGTC).

Statistics. Data are expressed as mean ± SEM. Statistical analysis was performed using 2-tailed Student's t test or ANOVA when appropriate to analyze statistically significant differences between groups. Log-rank analysis was used to compare differences in survival. Logarithmic values were used in the case of a skewed distribution. A P value of less than 0.05 is considered to be statistically significant.

Acknowledgments

We thank R.H. Adams (Max Planck Institute) for providing Pdgfrb-Cre mice, D. Holmyard (Mount Sinai Hospital) for electron microscopy, K. Harpal (SLRI) for histologic stainings, and D. White (University of Toronto) for FACS. This work was funded by CIHR grants MOP 77756 and 62931, NIH grant 1 U01 DK076136-01, Terry Fox grant TF016002 to S.E. Quaggin. S.E. Quaggin holds the Gabor-Zellerman Chair in Renal Research, UHN, University of Toronto, and is the recipient of a CRC Canada Research Chair Tier II. M. Henkelman holds a Tier I Canada Research Chair. M. Jeansson was funded by fellowships from Banting and Best Diabetes Centre and the Wenner-Gren Foundation. A. Gawlik was funded by the Rotation Program of RWTH University of Aachen.

Received for publication January 6, 2011, and accepted in revised form April 20, 2011.

Address correspondence to: Susan E. Quaggin, Samuel Lunenfeld Research Institute, Mount Sinai Hospital, 60 Murray Street, Box 41, Toronto, M4T 2Y4, Ontario, Canada. Phone: 416.586.4800, ext. 2859; Fax: 416.586.5130; E-mail: quaggin@lunenfeld.ca.

1. Satchell SC, Harper SJ, Tooke JE, Kerjaschki D, Saleem MA, Mathieson PW. Human podocytes express angiopoietin 1, a potential regulator of glomerular vascular endothelial growth factor. *J Am Soc Nephrol*. 2002;13(2):544–550.
2. Uemura A, et al. Recombinant angiopoietin-1 restores higher-order architecture of growing blood vessels in mice in the absence of mural cells. *J Clin Invest*. 2002;110(11):1619–1628.
3. Suri C, et al. Requisite role of angiopoietin-1, a ligand for the TIE2 receptor, during embryonic angiogenesis. *Cell*. 1996;87(7):1171–1180.
4. Partanen J, Dumont DJ. Functions of Tie1 and Tie2 receptor tyrosine kinases in vascular development. *Curr Top Microbiol Immunol*. 1999;237:159–172.
5. Tachibana K, Jones N, Dumont DJ, Puri MC, Bernstein A. Selective role of a distinct tyrosine residue on Tie2 in heart development and early hematopoiesis. *Mol Cell Biol*. 2005;25(11):4693–4702.
6. Fiedler U, et al. The Tie-2 ligand angiopoietin-2 is stored in and rapidly released upon stimulation from endothelial cell Weibel-Palade bodies. *Blood*. 2004;103(11):4150–4156.
7. Fiedler U, Augustin HG. Angiopoietins: a link between angiogenesis and inflammation. *Trends Immunol*. 2006;27(12):552–558.
8. van Meurs M, Kümpers P, Ligtenberg JJ, Meertens JH, Molema G, Zijlstra JG. Bench–to–bedside review: Angiopoietin signalling in critical illness – a future target? *Crit Care*. 2009;13(2):207.
9. Lim HS, Blann AD, Chong AY, Freestone B, Lip GY. Plasma vascular endothelial growth factor, angiopoietin-1, and angiopoietin-2 in diabetes: implications for cardiovascular risk and effects of multifactorial intervention. *Diabetes Care*. 2004;27(12):2918–2924.
10. Conroy AL, et al. Whole blood angiopoietin-1 and -2 levels discriminate cerebral and severe (non-cerebral) malaria from uncomplicated malaria. *Malar J*. 2009;8:295.

11. Nagy A. Cre recombinase: the universal reagent for genome tailoring. *Genesis*. 2000;26(2):99–109.
12. Visconti RP, Richardson CD, Sato TN. Orchestration of angiogenesis and arteriovenous contribution by angiopoietins and vascular endothelial growth factor (VEGF). *Proc Natl Acad Sci U S A*. 2002;99(12):8219–8224.
13. Brown LF, et al. Expression of vascular permeability factor (vascular endothelial growth factor) by epidermal keratinocytes during wound healing. *J Exp Med*. 1992;176(5):1375–1379.
14. Breyer MD, et al. Mouse Models of Diabetic Nephropathy. *J Am Soc Nephrol*. 2005;16(1):27–45.
15. Brosius FC III, et al. Mouse models of diabetic nephropathy. *J Am Soc Nephrol*. 2009; 20(12):2503–2512.
16. Eremina V, Wong MA, Cui S, Schwartz L, Quaggin SE. Glomerular-specific gene excision in vivo. *J Am Soc Nephrol*. 2002;13(3):788–793.
17. Foo SS, et al. Ephrin-B2 controls cell motility and adhesion during blood-vessel-wall assembly. *Cell*. 2006;124(1):161–173.
18. Eremina V, et al. Glomerular-specific alterations of VEGF-A expression lead to distinct congenital and acquired renal diseases. *J Clin Invest*. 2003; 111(5):707–716.
19. Eremina V, et al. VEGF inhibition and renal thrombotic microangiopathy. *N Engl J Med*. 2008; 358(11):1129–1136.
20. Satchell SC, Anderson KL, Mathieson PW. Angiopoietin 1 and vascular endothelial growth factor modulate human glomerular endothelial cell barrier properties. *J Am Soc Nephrol*. 2004;15(3):566–574.
21. Gavard J, Patel V, Gutkind JS. Angiopoietin-1 prevents VEGF-induced endothelial permeability by sequestering Src through mDia. *Developmental Cell*. 2008;14(1):25–36.
22. Thurston G, et al. Leakage-resistant blood vessels in mice transgenically overexpressing angiopoietin-1. *Science*. 1999;286(5449):2511–2514.
23. Armulik A, et al. Pericytes regulate the blood-brain barrier. *Nature*. 2010;468(7323):557–561.
24. Haraldsson B, Nystrom J, Deen WM. Properties of the glomerular barrier and mechanisms of proteinuria. *Physiol Rev*. 2008;88(2):451–487.
25. Sison K, et al. Glomerular structure and function require paracrine, not autocrine, VEGF-VEGFR-2 signaling. *J Am Soc Nephrol*. 2010;21(10):1691–1701.
26. Staton CA, Valluru M, Hoh L, Reed MW, Brown NJ. Angiopoietin-1, angiopoietin-2 and Tie-2 receptor expression in human dermal wound repair and scarring. *Br J Dermatol*. 2010;163(5):920–927.
27. Costa RA, Ruiz-de-Souza V, Azevedo Jr GM, Vaz NM, Carvalho CR. Effects of strain and age on ear wound healing and regeneration in mice. *Braz J Med Biol Res*. 2009;42(12):1143–1149.
28. Roberts AB, et al. Transforming growth factor type beta: rapid induction of fibrosis and angiogenesis in vivo and stimulation of collagen formation in vitro. *Proc Natl Acad Sci U S A*. 1986;83(12):4167–4171.
29. Cho CH, et al. COMP-angiopoietin-1 promotes wound healing through enhanced angiogenesis, lymphangiogenesis, and blood flow in a diabetic mouse model. *Proc Natl Acad Sci U S A*. 2006;103(13):4946–4951.
30. Cho C-H, et al. Long-term and sustained COMP-Ang1 induces long-lasting vascular enlargement and enhanced blood flow. *Circ Res*. 2005;97(1):86–94.
31. Vikkula M, et al. Vascular dysmorphogenesis caused by an activating mutation in the receptor tyrosine kinase TIE2. *Cell*. 1996;87(7):1181–1190.
32. Takakura N, Kidoya H. Maturation of blood vessels by haematopoietic stem cells and progenitor cells: involvement of apelin/APJ and angiopoietin/Tie2 interactions in vessel caliber size regulation. *Thromb Haemost*. 2009;101(6):999–1005.
33. Zhu Y, Lee C, Shen F, Du R, Young WL, Yang GY. Angiopoietin-2 facilitates vascular endothelial growth factor-induced angiogenesis in the mature mouse brain. *Stroke*. 2005;36(7):1533–1537.
34. Kim W, et al. COMP-Angiopoietin-1 Ameliorates Renal Fibrosis in a Unilateral Ureteral Obstruction Model. *J Am Soc Nephrol*. 2006;17(9):2474–2483.
35. Nakagawa T, Kosugi T, Haneda M, Rivard CJ, Long DA. Abnormal angiogenesis in diabetic nephropathy. *Diabetes*. 2009;58(7):1471–1478.
36. Eremina V, et al. Vascular endothelial growth factor a signaling in the podocyte-endothelial compartment is required for mesangial cell migration and survival. *J Am Soc Nephrol*. 2006;17(3):724–735.
37. Lee S, et al. Renoprotective effect of COMP-angiopoietin-1 in db/db mice with type 2 diabetes. *Nephrol Dial Transplant*. 2007;22(2):396–408.
38. Liu P, Jenkins NA, Copeland NG. A highly efficient recombineering-based method for generating conditional knockout mutations. *Genome Res*. 2003;13(3):476–484.
39. Joyner AL. *Gene Targeting A Practical Approach*. New York, New York, USA: Oxford University Press; 2000.
40. Dymecki SM. Flp recombinase promotes site-specific DNA recombination in embryonic stem cells and transgenic mice. *Proc Natl Acad Sci U S A*. 1996;93(12):6191–6196.
41. Walls JR, Coultas L, Rossant J, Henkelman RM. Three-dimensional analysis of vascular development in the mouse embryo. *PLoS One*. 2008;3(8):e2853.
42. Ema M, Takahashi S, Rossant J. Deletion of the selection cassette, but not cis-acting elements, in targeted Flk1-lacZ allele reveals Flk1 expression in multipotent mesodermal progenitors. *Blood*. 2006;107(1):111–117.